Method for spectral restoration of underwater images: theory and application

Yang Ping[1], Guo Yilu[2], Wei He[2], Song Dan[2], Song Hong[2], Zhang Yunfei[2], Shentu Yichun[2], Liu Hongbo[2], Huang Hui[2], Zhang Xiandou[1], Fang Meifen[3]

(1. School of Digital Media & Design, Hangzhou Dianzi University, Hangzhou 310018, China;
2. Ocean College, Zhejiang University, Zhoushan 316021, China;
3. Blue Science Opto-Electronics Co.Ltd., Hangzhou 310018, China)

Abstract: Underwater multispectral imaging is a promising technique for high-fidelity underwater color reproduction and mapping of kelp, sea grass, corals, etc. However, as light propagates through water, light is severely absorbed and scattered by water, causing image dim, hazy and distorted in its spectrum and color. In this paper, calibration of water attenuation coefficient based on underwater images and restoration of underwater multispectral images are discussed. Multispectral images of an underwater object are captured at different underwater distances. Technique has been proposed to calibrate the water attenuation coefficient based on underwater images of different distances and restore the raw images. Analysis was also conducted to search for the least number of distances for coefficient calibration and restoration. By comparing the restored underwater images with the images captured in air, it's found that the technique proposed in this paper provides accurate restoration of underwater spectral images, with a relative residual error of 5.87% in average for all test images.

Key words: multispectral imaging; water attenuation coefficient calibration; underwater image restoration

CLC number: TN95 **Document code:** A **DOI:** 10.3788/IRLA201746.0323001

一种用于水下图像的光谱重构方法:理论及应用

杨 萍[1],郭乙陆[2],魏 贺[2],宋 丹[2],宋 宏[2],张云菲[2],申屠溢醇[2],刘洪波[2],黄 慧[2],张显斗[1],方美芬[3]

(1. 杭州电子科技大学 数字媒体与艺术设计学院,浙江 杭州 310018;
2. 浙江大学 海洋学院,浙江 舟山 316021;
3. 杭州蓝科光电科技有限公司,浙江 杭州 310018)

摘 要: 多光谱成像是一项非常有前景的图像高保真获取与再现技术,近年来在水下物体颜色还原的应用中也受到的极大的需求和关注。然而,不同于空气中的物体的成像过程,在水下成像过程中,当光通过水而进行传播,光被水体严重吸收和散射,导致图像变暗,在其光谱和颜色方面发生

收稿日期:2016-07-05; **修订日期:**2016-08-03

基金项目:国家自然科学基金(61605038、11304278);国家高技术研究发展计划(2014AA093400)

作者简介:杨萍(1981-),女,讲师,博士,主要从事多光谱成像、颜色科学等方面的研究。Email:yangping@hdu.edu.cn

通讯作者:宋丹(1982-),男,讲师,博士,主要从事水下光学、流体动力学等方面的研究。Email:dsong@zju.edu.cn

模糊和扭曲。文中讨论的是基于水下图像的水衰减系数的校准和其多光谱图像的光谱重构。首先在不同的距离处获取物体的图像,提出了基于不同距离的图像进行水体衰减系数的校准并恢复原始图像的技术;在此基础上,分析并导出满足系数校准和图像复原所需的在不同距离获取到的最少的原始图像个数。最后,通过比较复原的水下图像与空气中获取的彩色图像,实验结果证明:文中提出的技术能够对水下光谱图像的进行精确颜色复原,所有测试图像的平均相对残留误差仅为 5.87%。

关键词:多光谱成像; 水衰减系数校准; 水下图像恢复

0 Introduction

Underwater multispectral imaging is a promising technique for high-fidelity underwater color reproduction and seafloor mapping[1], because the spectral images are able to provide "optical fingerprints" to objects being imaged. Although the technique has been used to map kelp[2], sea grass[3], corals[4] and near-shore habitats[5-6], it is still challenging to obtain spectral images of high accuracy or high fidelity in water, due to severe attenuation(e.g., absorption and scattering) of light by water[7-8]. The water attenuation on light is wavelength-dependent[9], which makes the calibration and restoration of underwater spectral images even more difficult.

Research has been conducted to compensate for the influence of water on underwater images. For instance, the water attenuation coefficient is measured by a dedicated instrument and the influence of water is compensated according to the Beer-Lambert law[1,10-13]. Panels with known spectral reflectance have been placed close to the underwater objects to be imaged, thus providing in-situ reference to the objects[11]. Besides, methods have also been proposed to correct the color of underwater images captured by 3-channel color cameras[14].

To highlight spectral features of the object from background, narrowband filters (typically with a full-width-half-maximum (FWHM) of no more than 10 nm) are desired so that images can be acquired at characteristic wavelengths or specific wavelengths of interest. Meanwhile, the complexity and accuracy of the calibration and restoration technique should be considered as well. Therefore in this paper, a technique is proposed to calibrate the water attenuation coefficient based on underwater spectral images captured by narrowband filters, without the need of any extra instrument to measure the water attenuation coefficient or placing any reference beside the underwater object. With the water attenuation coefficient calibrated, the underwater spectral images are then restored.

The paper is structured as follows. The spectral imaging system under investigation is described in Section 1. In Section 2, the technique on water attenuation coefficient calibration and image restoration is presented, followed by results and analysis in Section 3. The paper is concluded in Section 4.

1 System description

The system for imaging of underwater objects is shown in Fig.1, which consists of a narrowband multispectral imaging system, a water tank and a mobile phone inside a waterproof glass box.

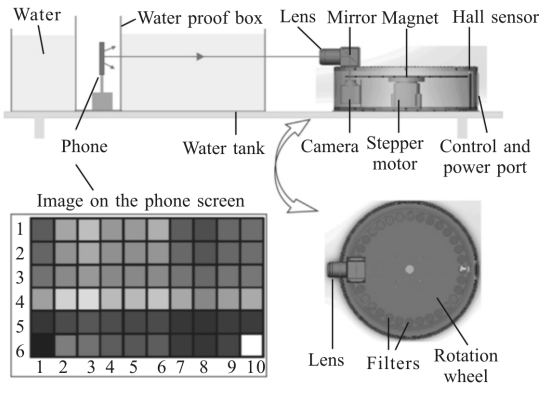

(a) Schematic of experimental setup

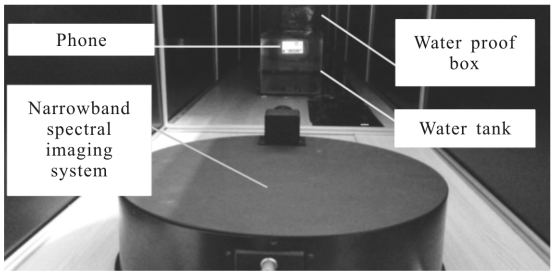

(b) Photo of experimental setup

Fig.1 A mobile phone is placed in a waterproof box, acting as a luminous underwater object. The pattern displayed in the screen of the phone consists of 60 color pieces in 6 rows and 10 columns. The filters in the multispectral imaging system is tuned by the rotation filter wheel with wavelength scanning from 420 nm to 700 nm at an interval of 20 nm

The multispectral imaging system mainly consists of an imaging lens, a mirror, a rotation filter wheel with a set of color filters and a monochrome CCD camera. The lens is a cemented doublet(GCL-010607, Daheng, China) with a focal length of 150 mm and a diameter of 38.1 mm. The filter wheel is rotated by a stepper motor. There are 15 bandpass color filters installed in the wheel. Beside each color filter, a tiny magnet is fixed to indicate the position of the color filter. The rotation angle of the wheel is monitored by a Hall sensor (together with the magnets in the wheel) and controlled by the computer. The color filters (FB serious, Thorlabs, USA) all have a FWHM of 10 nm, with the center wavelengths from 420 nm to 700 nm at an interval of 20 nm. The camera(Lm-165M, Lumenera, USA) has a resolution of 1 392 pixel×1 040 pixel and a dynamic range of 66 dB. During image acquisition, the filter wheel is rotated such that each color filter enters the imaging path successively and stays still in the light axis of the camera until the image is fully exposed.

The water tank (L300 cm×W30 cm×H30 cm) is made of 10 mm-thick quartz glass, filled with clean pipe water and placed in front of the spectral imaging system. The waterproof box (L35 cm×W25 cm×H50 cm) is made of 6-mm-thick quartz glass and placed inside the water tank. The waterproof box can be moved back and forth along the tank to change the distance to the spectral imaging system.

The mobile phone (Xiaomi 3, China) is placed inside the waterproof box, with 60 color pieces displayed on its screen, acting as the underwater object to be imaged. The screen pattern is specially designed for coefficient calibration. The color pieces are all squares in 6 rows and 10 columns so that the same color piece can be easily recognized when images are captured at different underwater distances or in air. Colors in each column have the same hue and ten columns just correspond to ten hues in the Munsell Color System[15], to cover a broad range of natural colors. Colors in each row are different combinations of values (lightness) and chromas (color purity). The black and white pieces in the left and right corners are used to extend the grayscale of the pattern.

2 Calibration and restoration

2.1 System analysis

The structure of the spectral imaging system is illustrated in Fig.2, where two situations are

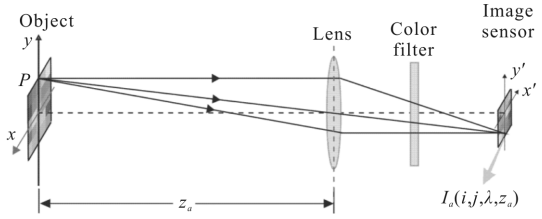

(a) Narrowband spectral imaging in air

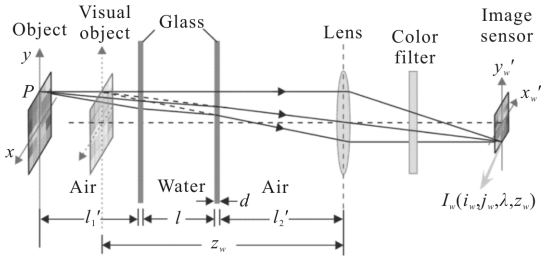

(b) Narrowband spectral imaging underwater

Fig.2 Illustration of narrowband spectral imaging in air and underwater

considered, i.e., imaging in air and imaging underwater. The main difference between these two situations lies in the spectral energy distortion due to water attenuation as well as the geometric distortion due to water refraction.

Referring to reference [13], the brightness of the image in air and underwater is related to each other as

$$I_w(i_w,j_w,\lambda,z_w)=\underbrace{\left(\frac{z_a}{z_a-f}\right)^2\cdot\left(\frac{z_w-f}{z_w}\right)^2\cdot I_a(i,j,\lambda,z_a)}_{I(i,j,\lambda,z)}\cdot \underbrace{\beta(\lambda)\mathrm{e}^{-\alpha(\lambda)l}}_{k(\lambda,l)}+\underbrace{\kappa(\lambda)\mathrm{e}^{-v(\lambda)l}+\gamma(\lambda)}_{b((\lambda,l))} \tag{1}$$

Where $I_w(i_w, j_w, \lambda, z_w)$ and $I_a(i, j, \lambda, z_a)$ are the image brightness of the same object captured in air and underwater, respectively; (i_w,j_w) and (i,j) are coordinates of the pixel in the image in air and underwater, respectively; λ is the wavelength of light. f is the focal length of lens. z_a is the object distance in air. z_w is the equivalent underwater distance defined as

$$z_w=\frac{l}{n_w}+\frac{d}{n_g}+l_1'+l_2' \tag{2}$$

Where l is the underwater distance; d is the thickness of the glass wall and l_1' and l_2' are the distances in air. n_w and n_g are refraction indices of water and glass, respectively.

The term

$$I(i,j,\lambda,z)=\left(\frac{z_a}{z_a-f}\right)^2\cdot\left(\frac{z_w-f}{z_w}\right)^2\cdot I_a(i,j,\lambda,z_a) \tag{3}$$

counts for the change in the image brightness due to water refraction and the difference in object distance.

The effect of water attenuation is represented in the terms $k(\lambda, l)$ and $b(\lambda, l)$, where $\alpha(\lambda)$ is the attenuation coefficient of water, $\beta(\lambda)$ is the total transmissivity of the water-glass-air interface, $\kappa(\lambda)\mathrm{e}^{-v(\lambda)l}$ is the hazing factor with coefficients $\kappa(\lambda)$ and $v(\lambda)$. The influence of stray light and voltage in the image sensor is involved in $\gamma(\lambda)$.

2.2 Coefficients calibration and restoration

To compensate for the influence of water attenuation and restore underwater images, all the coefficients in $k(\lambda, l)$ and $b(\lambda, l)$ should be identified, i.e. $\alpha(\lambda)$, $\beta(\lambda)$, $\kappa(\lambda)$, $v(\lambda)$, $\gamma(\lambda)$. In this paper, an image-based calibration technique is proposed as no extra hardware is required and the calibrated coefficients can be directly used for image restoration.

For each color piece displayed in the screen of the mobile phone, an equation can be formed as in Eq. (1) to relate the underwater image brightness to the image brightness in air and distance .

There′re 60 color pieces in the pattern, a set of equations can be formed as

$$\begin{cases} I_w(i_{w,1},j_{w,1},\lambda_1,z_{w,1})=k(\lambda_1,l_1)I(i_1,j_1,\lambda_1,z_1)+b(\lambda_1,l_1) \\ I_w(i_{w,2},j_{w,2},\lambda_1,z_{w,1})=k(\lambda_1,l_1)I(i_2,j_2,\lambda_2,z_2)+b(\lambda_1,l_1) \\ \quad\vdots\qquad\quad\vdots\qquad\qquad\vdots \\ I_w(i_{w,6},j_{w,10},\lambda_1,z_{w,1})=k(\lambda_1,l_1)I(i_6,j_{10},\lambda_1,z_1)+b(\lambda_1,l_1) \end{cases} \tag{4}$$

Where the calibration pattern is imaged both in air and underwater, with an underwater distance of l_1 and object distance of z_1 in air. The wavelength for image acquision is denoted as λ_1, without losing generality.

Write Eq. (4) in matrix form, then we have a compact matrix equation as

$$\underbrace{\begin{bmatrix} I(i_1,j_1,\lambda_1,z_1) & 1 \\ I(i_2,j_2,\lambda_2,z_2) & 1 \\ \vdots & \vdots \\ I(i_6,j_{10},\lambda_1,z_1) & 1 \end{bmatrix}}_{B}\cdot\underbrace{\begin{bmatrix} k(\lambda_1,l_1) \\ b(\lambda_1,l_1) \end{bmatrix}}_{X}=\underbrace{\begin{bmatrix} I_w(i_{w,1},j_{w,1},\lambda_1,z_{w,1}) \\ I_w(i_{w,2},j_{w,2},\lambda_1,z_{w,1}) \\ \vdots \\ I_w(i_{w,6},j_{w,10},\lambda_1,z_{w,1}) \end{bmatrix}}_{Y} \tag{5}$$

Terms $k(\lambda_1,l_1)$ and $b(\lambda_1,l_1)$ can be estimated using linear least squares (LLS) method as

$$\hat{X}=(B^{\mathrm{T}}B)^{-1}B^{\mathrm{T}}Y \tag{6}$$

Where $\hat{X}$ is the estimate of the unknown vector X.

Suppose we have images captured different distances, namely l_1, l_2, …, l_M, then another two sets of equations can be formed as

$$\beta(\lambda_1)=\underbrace{\begin{bmatrix} \mathrm{e}^{-\alpha(\lambda_1)l_1} \\ \mathrm{e}^{-\alpha(\lambda_1)l_2} \\ \vdots \\ \mathrm{e}^{-\alpha(\lambda_1)l_M} \end{bmatrix}}_{P(\alpha)}=\underbrace{\begin{bmatrix} k(\lambda_1,l_1) \\ k(\lambda_1,l_2) \\ \vdots \\ k(\lambda_1,l_M) \end{bmatrix}}_{K} \tag{7}$$

$$\kappa(\lambda_1)=\underbrace{\begin{bmatrix} \mathrm{e}^{-v(\lambda_1)l_1} \\ \mathrm{e}^{-v(\lambda_1)l_2} \\ \vdots \\ \mathrm{e}^{-v(\lambda_1)l_M} \end{bmatrix}}_{Q(v)}+\gamma(\lambda_1)=\underbrace{\begin{bmatrix} b(\lambda_1,l_1) \\ b(\lambda_1,l_2) \\ \vdots \\ b(\lambda_1,l_M) \end{bmatrix}}_{Z} \tag{8}$$

According to the definition of $k(\lambda,l)$ and $b(\lambda,l)$

in Eq.(1), unknown coefficients $\alpha(\lambda_1)$, $\beta(\lambda_1)$, $v(\lambda_1)$, $\kappa(\lambda_1)$ and $\gamma(\lambda_1)$ can be estimated by solving an optimization problem as

$$\hat{\alpha}(\lambda_1),\hat{\beta}(\lambda_1)=\underset{\alpha^*,\beta^*}{\operatorname{argmin}} \underbrace{\|K-\beta^* P(\alpha^*)\|_2^2}_{J} \tag{9}$$

$$\hat{v}(\lambda_1),\hat{\kappa}(\lambda_1),\hat{Y}(\lambda_1)=\underset{v^*,\kappa^*,\gamma^*}{\operatorname{argmin}} \underbrace{\|Z-\gamma^*-\kappa^* Q(v^*)\|_2^2}_{J'} \tag{10}$$

where $\hat{\alpha}(\lambda_1)$, $\hat{\beta}(\lambda_1)$, $\hat{v}(\lambda_1)$, $\hat{\kappa}(\lambda_1)$ and $\hat{\gamma}(\lambda_1)$ are the estimates of $\alpha(\lambda_1)$, $\beta(\lambda_1)$, $v(\lambda_1)$, $\kappa(\lambda_1)$ and $\gamma(\lambda_1)$, respectively. J and J' are the cost functions (also called objective functions) to be minimized by optimization algorithm.

With coefficients $\hat{\alpha}(\lambda_1)$, $\hat{\beta}(\lambda_1)$, $\hat{v}(\lambda_1)$, $\hat{\kappa}(\lambda_1)$ and $\hat{\gamma}(\lambda_1)$ available, the underwater images can be restored as

$$\hat{I}_c(i,j,\lambda_1,z_1)=\frac{I_w(i,j,\lambda_1,z_1)-\hat{b}(\lambda_1,l_1)}{\hat{k}(\lambda_1,l_1)} \tag{11}$$

where $\hat{I}_c(i,j,\lambda_1,z_1)$ is the brightness of restored image. $\hat{k}(\lambda_1,l_1)$ and $\hat{b}(\lambda_1,l_1)$ are estimates of $k(\lambda_1,l_1)$ and $b(\lambda_1,l_1)$, respectively, calculated as

$$\hat{k}(\lambda_1,l_1)=\hat{\beta}(\lambda_1)\mathrm{e}^{-\hat{\alpha}(\lambda_1)l_1} \tag{12}$$

$$\hat{b}(\lambda_1,l_1)=\hat{\kappa}(\lambda_1)\mathrm{e}^{-\hat{v}(\lambda_1)l_1}+\gamma(\lambda_1) \tag{13}$$

2.3 Underwater distance selection

The accuracy of coefficient calibration depends on not only the number of underwater images for calibration, but also on the underwater distances where the images are captured.

The number of underwater images determines the number of equations used for optimization. In general, the more equations are involved, the more accurate the optimization will be.

The range of underwater distances determines the applicability of the calibrated coefficients for image restoration. To achieve accurate restoration, the calibration distances should be as close to those for image restoration. However, in practice, as limited by the time, the availability and capability of underwater equipments and accessibility of the underwater environment to be imaged, it can′t be guaranteed that the calibration distances cover exactly that for restoration. Therefore it′s important to evaluate the consequence if the restoration distances are not covered during calibration and the minimum number of distances for efficient calibration.

As will be described in Section 3, underwater images captured within an underwater range of [0, 260 cm] will be restored. Four cases are considered for the calibration distances, concerning the distance range. In each case, the number of distances is increased to evaluate its effect on image restoration.

Case 1: Only images captured at short distances are used for calibration, e.g., images captured at {10 cm, 20 cm, 30 cm}, {10 cm, 20 cm, 30 cm, 40 cm}.

Case 2: Only images captured at long distances are used for calibration, e.g., images captured at {260 cm, 250 cm, 240 cm}, {260 cm, 250 cm, 240 cm, 230 cm}.

Case 3: Only images captured at medium distances are used for calibration, e.g., images captured at {120 cm, 130 cm, 140 cm}, {120 cm, 130 cm, 140 cm, 150 cm}.

Case 4: Calibration distances cover the same range as restoration, but only the number of distances is changed, e.g., {10 cm, 130 cm, 250 cm}, {10 cm, 90 cm, 180 cm, 250 cm}.

The accuracy of coefficient calibration and image restoration will be evaluated for each case and for different number of distances.

3 Experiments and results

3.1 Experiments

Experiments are carried out in the setup shown in Fig.1. To avoid overexposed or dark images, a scan of the multispectral images of the phone screen is conducted for different wavelength and underwater distances before image acquisition, during which the exposure time is set from 50 ms to 500 ms, and the most appropriate exposure time for each wavelength and distance is determined. One multispectral image cube is acquired in air at a fixed distance of 340 cm and 26 multispectral image cubes are acquired

underwater for underwater distances of 10 cm, 20 cm, ..., 260 cm, respectively. Each image cube (both in air and underwater) consists of 15 images captured at wavelengths of 420 nm, 440 nm, ..., 700 nm, respectively.

Preprocessing are conducted to correct the geometric distortion and the brightness of all images is normalized to an exposure tine of 50 ms.

3.2 Coefficient calibration

Coefficient calibration follows the steps described in Section 2. The choice of calibration distances is very important for image restoration. Therefore four cases are considered and the results are compared.

Intermediate terms $k(\lambda,l)$ and $b(\lambda,l)$ are calculated as in Eqs.(5) and (6), based on the images of 60 color pieces captured in air and underwater at certain wavelength and distance. With $k(\lambda,l)$ and $b(\lambda,l)$ available at several underwater distances, the coefficients $\alpha(\lambda)$, $\beta(\lambda)$, $v(\lambda)$, $\kappa(\lambda)$ and $\gamma(\lambda)$ are estimated as in Eqs.(9) and (10). Figure 3 shows the fitting curves when different underwater distances are selected to optimize the parameters $\alpha(\lambda)$, $\beta(\lambda)$, $v(\lambda)$, $\kappa(\lambda)$ and $\gamma(\lambda)$ at a wavelength of 520 nm. It can be seen that the results differ for 4 cases. Particularly, the fitting curve in case 2 (i.e., distant images are selected) deviates from the original data severely. This is mainly due to the low image brightness in images faraway. The difference in $b(\lambda, l)$ is quite apparatus when different distances are selected. This may be due to the fact that there are 3 unknowns to be estimated in $b(\lambda,l)$ while only 2 in $k(\lambda,l)$, and $b(\lambda,l)$ is about two order of magnitude smaller than $k(\lambda,l)$, thus the optimization process of $b(\lambda, l)$ is more sensitive to small disturbance or noise.

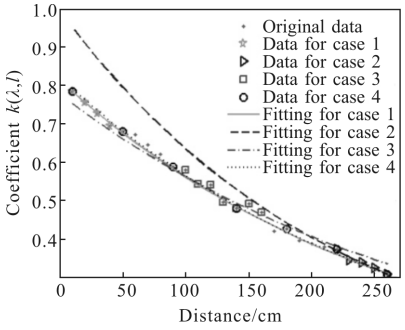

(a) Fitting for $k(\lambda,l)$ with 6 underwater distances

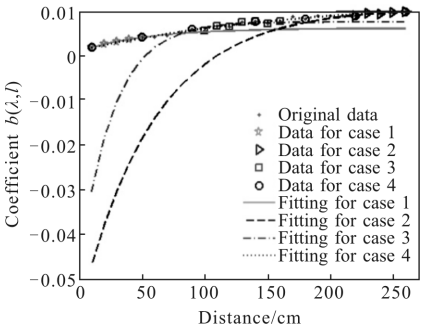

(b) Fitting for $b(\lambda,l)$ with 6 underwater distances

Fig.3 Exponential fitting of $k(\lambda,l)$ and $b(\lambda,l)$ to estimate unknown coefficients

Figure 4 shows the relative estimation error of $k(\lambda,l)$ and $b(\lambda,l)$ with respect to the number of distances, averaged over all 15 wavelengths. The difference between 4 cases is quite significant, especially when only a small number of distances are involved. In general, as more distances are used for optimization, the results converge and become more accurate.

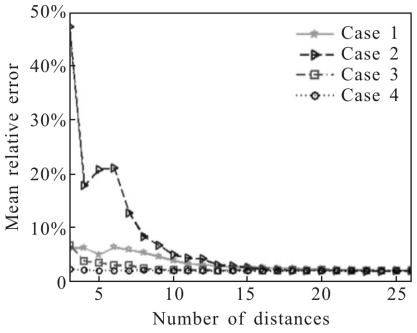

(a) Mean relative estimation error in $k(\lambda,l)$

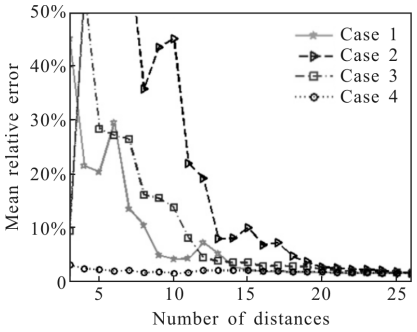

(b) Mean relative estimation error in $b(\lambda,l)$

Fig.4 Mean relative estimation error of residual of $k(\lambda,l)$ and $b(\lambda,l)$

3.3 Restoration

With the coefficients calibrated, underwater

multispectral images are restored and color images are reconstructed.

Figure 5 shows the restoration error of four cases for the spectral images captured at a wavelength of 520 nm. The raw images, restored images and images captured in air are compared in Fig.6. It is clearly visible that underwater images are very dim image intensity and shade color, while the restored images, have brightness close to that captured in air. Calibration with equally separated distances provides the best results with a relative residual error of 5.87% for all test images. A Sub-optimal choice is to use short-distance or medium-distance images, while the coefficients calibrated from distant images lead to largest deviation in the restored images.

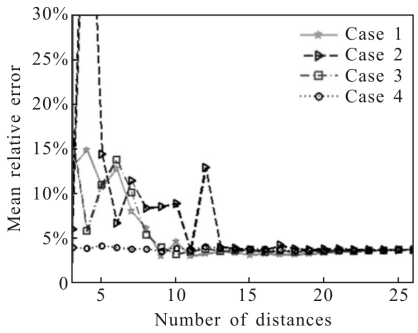

Fig.5 Restoration error of images at a wavelength of 520 nm in 4 cases

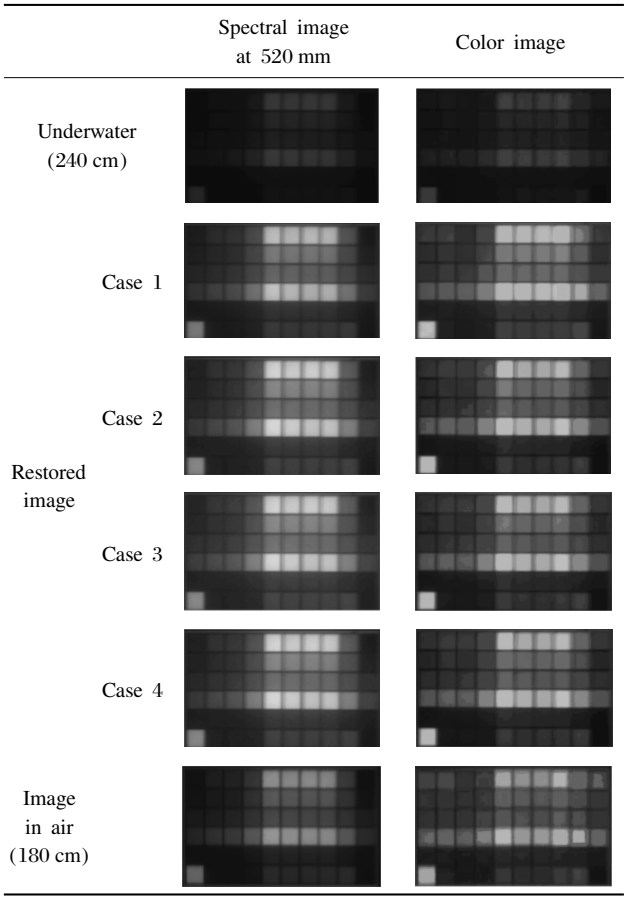

Fig.6 Comparison among raw underwater images, restored underwater images in different case and air images. Color images are constructed from spectral images

4 Conclusion

Technique on calibration and restoration of spectral images for underwater objects has been proposed in this paper. Experimental results show that a relative restoration error of 5.87% is achieved when the coefficients for restoration are calibrated accurately with equally-spaced underwater images.

Future work will focus on the development of the underwater spectral image system.

References:

[1] Johnsen G, Volent Z, Dierssen H, et al. 20 –Underwater hyperspectral imagery to create biogeochemical maps of seafloor properties [J]. ***Journal of Engineering Physics and Thermophysics***, 2010, 83(3):508–535.

[2] Volent A Z, Johnsen G, Sigernes F. Kelp forest mapping by use of airborne hyperspectral imager [J]. ***Journal of Applied Remote Sensing***, 2007, 1(1):6656–6659.

[3] Dierssen H M, Zimmerman R C, Drake L A, et al. Benthic ecology from space: optics and net primary production in seagrass and benthic algae across the great bahama bank[J]. ***Marine Ecology Progress***, 2010, 411(6): 1–15.

[4] Gleason A C R, Gracias N, Lirman D, et al. Landscape video mosaic from a mesophotic coral reef [J]. ***Coral Reefs***, 2010, 29(2):253–253.

[5] Aarrestad S M. Use of underwater hyperspectral imagery for geological characterization of the seabed [D]. Trondheim: NTNU, 2014.

[6] Sakshaug E, Johnsen G H, Kovacs K M. Ecosystem Barents Sea[M]. Norway: Tapir Academic Pres, 2009.

[7] Mumby P J, Clark C D, Green E P, et al. Benefits of water column correction and contextual editing for mapping coral

reefs[J]. ***International Journal of Remote Sensing***, 1998, 19 (1): 203-210.

[8] Holden H, Ledrew E. Effects of the water column on hyperspectral reflectance of submerged coral reef features[J]. ***Bulletin of Marine Science -Miami-***, 2001, 69(2): 685-699.

[9] Raymond C S, Karen S B. Optical properties of the clearest natural waters (200-800 nm)[J]. ***Applied Optics***, 1981, 20 (2): 177-184.

[10] Moore C, Barnard A, Fietzek P, et al. Optical tools for ocean monitoring and research [J]. ***Ocean Science***, 2009, 5 (5): 661-684.

[11] Gleason A C R, Reid R P, Voss K J. Automated classification of underwater multispectral imagery for coral reef monitoring[C]//OCEANS, IEEE, 2007: 1-8.

[12] Mishra D R, Narumalani S, Rundquist D, et al. Characterizing the vertical diffuse attenuation coefficient for downwelling irradiance in coastal waters: Implications for water penetration by high resolution satellite data [J]. ***Isprs Journal of Photogrammetry & Remote Sensing***, 2005, 60 (1): 48-64.

[13] Guo Y, Song H, Liu H, et al. Model-based restoration of underwater spectral images captured with narrowband filters [J]. ***Optics Express***, 2016, 24(12): 13101.

[14] Ahlen J. Colour correction of underwater images using spectral data [D]. Uppsala: Acta Universitatis Upsaliensis, 2005.

[15] Munsell A H. A Color Notation [M]. Baltimore: Munsell Color Company Inc., 1905.